Collective coordinates and an accompanying metric force in structural isomerization dynamics of molecules

Tomohiro Yanao* and Kazuo Takatsuka†
Department of Basic Science, Graduate School of Arts and Sciences, University of Tokyo, Komaba, 153-8902 Tokyo, Japan
(Received 6 November 2002; published 17 September 2003)

Structural isomerization dynamics of three- and four-atom clusters of vanishing total angular momentum is studied in terms of internal coordinates of *n*-body systems on the basis of a gauge theory. The so-called principal-axis hyperspherical coordinates are employed effectively as collective variables for the study of isomerization reactions. It turns out that the non-Euclidean metric on the internal space gives rise to a force, which works in response to internal motions called the democratic (kinematic) rotations in the internal space. This metric force generally tends to induce an asymmetry in mass balance of a system, and is coupled with the usual potential force to give rise to trapped motions in the vicinity of the transition states of the cluster. This observation provides a different perspective for the so-called recrossing problem in chemical reaction dynamics.

DOI: 10.1103/PhysRevA.68.032714 PACS number(s): 34.10.+x, 02.40.−k, 36.40.−c, 33.20.Vq

I. INTRODUCTION

Large-amplitude collective motions are ubiquitous in many-body systems such as atomic, nuclear, and also in celestial systems, and understanding of the fundamental principles for their mechanisms is crucial in many fields of current science. Internal rearrangement of nonrigid molecules is one of such typical collective motions, much of which is still open. As an archetypal example, the structural isomerization dynamics of van der Waals clusters together with its thermodynamical properties is quite interesting and has been extensively investigated by many authors from various points of view; as a microcanonical analog of the first-order solid-liquid phase transition [1,2], as the Hamiltonian systems where chaotic and relatively regular dynamics coexist [3–5], as a dynamics on complicated potential-energy hypersurface [6], and as a prototype of high-energy multichannel chemical reactions [7].

Most of the past studies in chemical dynamics, however, seem to have concentrated on the topography of potential-energy hypersurfaces to extract the origin of collective internal motions. For instance, the traditional reaction-rate theories, such as the transition-state theory [8,9], assume more or less separability of the internal and orientational degrees of freedom, isolating the dynamics on the potential-energy hypersurface from kinematics arising from the molecular frames. It is a usual practice to obtain the space for internal motions of a polyatomic molecule by reducing the overall translational and rotational degrees of freedom from the entire $3n$ dimensional space, where n is the number of constituent atoms. In isomerization dynamics, however, it is critically important to recognize the very basic issue of how the space for internal motions is constructed. Although the elimination of the translational degrees of freedom is trivial, the separation of rotational and internal coordinates is not. The problem of the so-called ''falling cat'' demonstrates this situation very clearly [10,11]; a falling cat can turn itself over without generating angular momentum. Similar effect can also be seen in our molecular systems: If a polyatomic molecule changes its shape continuously and returns to the initial shape keeping the total angular momentum to zero, the final orientation of the molecule can be generally different from the initial one, and it depends on the history of way of changing the molecular shape. The molecular shape is usually viewed with respect to a body frame, but the body frame itself changes as a result of the molecular deformation. This is true even for a system of zero angular momentum. Therefore, a very careful treatment of the body frame is crucial to quantify the internal motions of a polyatomic system.

As a consequence of nonuniqueness to determine a body frame, an associated gauge field arises inevitably in the internal space. The gauge theory arising from separation between rotation and internal motion of a polyatomic molecule has been developed by Guichardet [12], Tachibana, and Iwai [13,14]. These authors have developed an idea that regards the translation-reduced configuration space as a principal fiber bundle with rotational structure group. The fiber-bundle view of configuration space sets a theoretical basis for precise treatment of rotational and internal motions of deformable bodies. More recently, Littlejohn and Reinsch [11] have presented a systematic theory on the separation of rotations and internal motions. Their study is quite suggestive to the study of isomerization dynamics in which it is demonstrated that the Euclidean metric on the configuration space and the gauge field are coupled to induce a non-Euclidean metric on the internal space. It seems that this intrinsically curved nature of internal space has not been fully appreciated in the past studies on large-amplitude collective motions of polyatomic molecules and in chemical reaction dynamics. We here explore the significance of the intrinsic metric structure of internal space in the collective isomerization dynamics of small clusters.

Our first subject is to find an appropriate body frame that should be referred to and an appropriate coordinate system in internal space, on the basis of which one can describe the

*Electronic address: yanao@mns2.c.u-tokyo.ac.jp
†Electronic address: kaztak@mns2.c.u-tokyo.ac.jp

collective isomerization dynamics systematically, accounting for the effect of the non-Euclidean metric upon the dynamics. As for a body frame, rotation of the principal axes of instantaneous moment-of-inertia tensor of a molecule should reflect the change of the molecular shape. On the other hand, the idea behind the so-called hyperspherical coordinates is quite attractive for the large-amplitude motions since these coordinates treat each atom in a ''democratic manner'' [15] in terms of the hyperangles. With these basic ideas in mind, we here adopt a coordinate system called the principal-axis hyperspherical coordinates (PAHC), which was initially suggested by Eckart [16] and recently developed by Chapuisat *et al.* [17–19] and Kuppermann [20]: A time-dependent body frame is first determined referring to the principal axes of the instantaneous moment-of-inertia tensor of a nonrigid molecule, and then the PAHC is defined accordingly on the internal space using the hyperangles and the gyration radii, the latter representing the mass-weighted length of a molecule along each principal axis. The hyperangles parametrize the symmetry group of the metric tensor in the internal space. The change of the hyperangles is referred to as kinematic rotation or democratic rotation, which generates a cyclic and democratic deformation of molecular shape. The geometry of the democratic rotations in internal space and the related singularities of the body frames have been scrutinized by Littlejohn *et al.* [21–23]. The cyclic internal motions in a molecule should have a universal significance in many-body dynamics. For instance, it is closely related to the pseudorotations of nonrigid molecule which are often discussed in the literature of stereochemistry [24] and of Berry's geometrical phase [25,26].

As a significant effect of the intrinsic non-Euclidean metric in the internal space represented in terms of the PAHC, arises a ''centrifugal force,'' which we call the democratic centrifugal force (DCF). DCF is induced in the space of gyration radii as a result of the democratic rotation. It is different from the usual centrifugal force in that it is an internal force and generated even in a system of zero angular momentum. It is found that the DCF plays quite a dominant role in isomerization dynamics. For instance, the DCF tends to deform a molecular shape so as to avoid a degeneracy between two of the gyration radii. This effect is rather analogous to the Jahn-Teller effects [27], in which the electronic degeneracy is broken by a distortion of the molecular shape. Further, we will show that the DCF gives a theoretical foundation of ''trapped'' motion in vicinity of the so-called transition states and sheds a new light on the well-known recrossing problem, which has been studied in the theory of chemical reaction dynamics for a couple of decades [28,29].

The present paper is organized as follows. In Sec. II, we summarize a minimum description of the general gauge-theoretical formalism in a manner similar to the review by Littlejohn and Reinsch [11]. In Sec. III, after introducing our model cluster, we employ a gauge convention that refers to the principal-axis frame and show explicitly the PAHC for a three-atom cluster. With this scheme, the mechanism of structural isomerization of three-atom cluster is clarified numerically and the role of the democratic centrifugal force is highlighted. In Sec. IV, we investigate a four-atom cluster with zero angular momentum by extending the method of Sec. III. We will see the essential similarity between three- and four-atom clusters. This paper concludes in Sec. V with some remarks.

II. GAUGE-THEORETICAL FORMALISM FOR INTERNAL MOTIONS OF GENERAL *n*-BODY SYSTEMS OF VANISHING ANGULAR MOMENTUM

To present the main results of this paper, this section summarizes a minimum amount of the gauge-theoretical formalism for the *n*-body problem [11].

A. Orientational and internal freedoms: Gauge-dependent descriptions

Let the mass of the ith particle and its position with respect to an origin be m_i and $\boldsymbol{r}_{si}$ $(i=1,\ldots,n)$, respectively, where $\boldsymbol{r}_{si}$ is the usual three-dimensional column vector. The subscript s on $\boldsymbol{r}_{si}$, and on other quantities as well, indicates a vector relative to a space-fixed frame, whereas a vector $\boldsymbol{r}_i$ without subscript s represents a position vector relative to a body frame throughout this paper. To remove the translational degrees of freedom from the Hamiltonian, we employ the mass-weighted Jacobi coordinates $\{\boldsymbol{\rho}_{s1},\boldsymbol{\rho}_{s2},\ldots,\boldsymbol{\rho}_{sn-1}\}$, which constitute an Euclidean space [11,30].

The translation-reduced configuration space can be regarded as a principal fiber bundle with structure group SO(3), if the singular configurations such as collinear configurations are removed [11–14] . Let a body frame (body-fixed frame) be represented by a 3×3 proper rotation matrix $\mathsf{R}\in\mathrm{SO}(3)$, whose three columns represent the three orthonormal axes of the frame. Origin of the body frame is fixed to the center of mass of the system. The body frame R specifies orientation of the *n*-body system and may be parametrized by the three Euler angles $\{\theta^{\xi}\}$ $(\xi=1,2,3)$. The body frame should be assigned for each configuration of the system continuously according to a certain rule, which corresponds to the gauge convention in the gauge-theoretical formalism. In Sec. III, we will specify the body frame in a concrete manner. If a body frame is defined, the mass-weighted Jacobi vectors referred to this frame $\{\boldsymbol{\rho}_i\}$ are related to $\{\boldsymbol{\rho}_{si}\}$ by

$$\boldsymbol{\rho}_{si}=\mathsf{R}(\{\theta^{\xi}\})\boldsymbol{\rho}_i(\{q^{\mu}\}) \quad (i=1,\ldots,n-1), \tag{1}$$

where $\{\boldsymbol{\rho}_i\}$ are the functions of $3n-6$ internal coordinates $\{q^{\mu}|\mu=1,\ldots,3n-6\}$. The internal space having these coordinates is invariant under rotation of the system.

Differentiating Eq. (1) with respect to time, we obtain the velocity vector $\dot{\boldsymbol{\rho}}_{si}$

$$\dot{\boldsymbol{\rho}}_{si}=\dot{\mathsf{R}}\boldsymbol{\rho}_i+\mathsf{R}\frac{\partial\boldsymbol{\rho}_i}{\partial q^{\mu}}\dot{q}^{\mu}, \tag{2}$$

where the sum convention is adopted for the index μ from 1 to $3n-6$. Likewise, we always adopt this convention for the greek indices such as μ, ν, and so on. The angular momentum referred to the body frame $\boldsymbol{L}=\mathsf{R}^T\boldsymbol{L}_s$ (T on the shoulder

indicating the transposition, and $\boldsymbol{L}_s=\Sigma_{i=1}^{n-1}\boldsymbol{\rho}_{si}\times\dot{\boldsymbol{\rho}}_{si}$ being the angular momentum with respect to the space-fixed frame) is

$$\boldsymbol{L}=\mathsf{R}^T\sum_{i=1}^{n-1}\boldsymbol{\rho}_{si}\times\dot{\boldsymbol{\rho}}_{si}=\sum_{i=1}^{n-1}\boldsymbol{\rho}_i\times(\boldsymbol{\omega}\times\boldsymbol{\rho}_i)+\sum_{i=1}^{n-1}\boldsymbol{\rho}_i\times\frac{\partial\boldsymbol{\rho}_i}{\partial q^\mu}\dot{q}^\mu, \tag{3}$$

where we have defined the angular velocity vector $\boldsymbol{\omega}$ of the body frame that is referred to the frame itself. The three-dimensional vector $\boldsymbol{\omega}$ has a correspondence to the angular velocity matrix Ω in a manner that

$$\Omega\equiv\mathsf{R}^T\dot{\mathsf{R}}=\begin{pmatrix}0&-\omega_3&\omega_2\\ \omega_3&0&-\omega_1\\ -\omega_2&\omega_1&0\end{pmatrix}\Leftrightarrow\boldsymbol{\omega}\equiv\begin{pmatrix}\omega_1\\ \omega_2\\ \omega_3\end{pmatrix}. \tag{4}$$

Equation (3) can be rewritten as

$$\boldsymbol{L}=\mathsf{M}(\boldsymbol{\omega}+\boldsymbol{A}_\mu\dot{q}^\mu), \tag{5}$$

where M is the moment-of-inertia tensor referred to the body frame, whose components are

$$M_{\alpha\beta}=\sum_{i=1}^{n-1}[(\boldsymbol{\rho}_i\cdot\boldsymbol{\rho}_i)\delta_{\alpha\beta}-\rho_{i\alpha}\rho_{i\beta}], \tag{6}$$

where α and β correspond to the axes of the body frame and $\delta_{\alpha\beta}$ is the Kronecker delta. $\boldsymbol{A}_\mu$ in Eq. (5) is the gauge potential defined by

$$\boldsymbol{A}_\mu=\mathsf{M}^{-1}\left(\sum_{i=1}^{n-1}\boldsymbol{\rho}_i\times\frac{\partial\boldsymbol{\rho}_i}{\partial q^\mu}\right). \tag{7}$$

The kinetic energy in the Jacobi coordinates is then represented in terms of the quantities referred to the body frame as

$$K=\frac{1}{2}(\boldsymbol{\omega}^T\mathsf{M}\boldsymbol{\omega})+(\boldsymbol{\omega}^T\mathsf{M}\boldsymbol{A}_\mu)\dot{q}^\mu+\frac{1}{2}h_{\mu\nu}\dot{q}^\mu\dot{q}^\nu, \tag{8}$$

where $h_{\mu\nu}$ is a metric defined by

$$h_{\mu\nu}=\sum_{i=1}^{n-1}\frac{\partial\boldsymbol{\rho}_i}{\partial q^\mu}\cdot\frac{\partial\boldsymbol{\rho}_i}{\partial q^\nu}. \tag{9}$$

The second term on the right-hand side of Eq. (8) is known as the Coriolis term. But none of the three terms in the right-hand side of Eq. (8) is individually gauge invariant, that is, the decomposition of kinetic energy in Eq. (8) depends on the choice of the body frame.

B. Gauge-invariant metric of internal space and dynamics in it

The metric $h_{\mu\nu}$ in Eq. (9) does not give an appropriate description of internal motions because of the lack of gauge invariance. $h_{\mu\nu}$ is therefore referred to as the pseudo-metric tensor. Littlejohn and Reinsch [11] have presented a way of obtaining a gauge-invariant metric tensor on the internal space by rearranging the kinetic energy of Eq. (8) into a gauge-invariant form based on the fiber-bundle picture of configuration space. The result has been formulated as

$$K=\frac{1}{2}(\boldsymbol{\omega}+\boldsymbol{A}_\mu\dot{q}^\mu)^T\mathsf{M}(\boldsymbol{\omega}+\boldsymbol{A}_\nu\dot{q}^\nu)+\frac{1}{2}g_{\mu\nu}\dot{q}^\mu\dot{q}^\nu, \tag{10}$$

where $g_{\mu\nu}$ is defined as

$$g_{\mu\nu}=h_{\mu\nu}-\boldsymbol{A}_\mu^T\mathsf{M}\boldsymbol{A}_\nu. \tag{11}$$

The first and the second terms in the right-hand side of Eq. (10) are gauge invariant individually. The metric tensor $g_{\mu\nu}$, which is also gauge invariant, is called the true metric in the internal space. It should be noted that $g_{\mu\nu}$ is not Euclidean for n-body systems in general. Calculation of $g_{\mu\nu}$ for a desired coordinate system constitutes one of the fundamental subjects in what follows.

The first term in the right-hand side of Eq. (10) vanishes if and only if the total angular momentum $\boldsymbol{L}$ is zero [cf. Eq. (5)]. The Lagrangian is then reduced to

$$\mathcal{L}=\frac{1}{2}g_{\mu\nu}\dot{q}^\mu\dot{q}^\nu-V(\{q^\mu\}). \tag{12}$$

Here we restrict ourselves to the case that the potential energy V of the system depends only on the internal coordinates $\{q^\mu\}$. The classical equations of motion are obtained from this Lagrangian by applying the Euler-Lagrange variational principle, with the result being

$$g_{\mu\nu}(\ddot{q}^\nu+\Gamma^\nu_{\kappa\lambda}\dot{q}^\kappa\dot{q}^\lambda)=-\frac{\partial V}{\partial q^\mu}, \tag{13}$$

where the Christoffel symbols $\Gamma^\nu_{\kappa\lambda}$ are given by

$$\Gamma^\nu_{\kappa\lambda}=\frac{1}{2}g^{\nu\mu}\left(\frac{\partial g_{\mu\kappa}}{\partial q^\lambda}+\frac{\partial g_{\mu\lambda}}{\partial q^\kappa}-\frac{\partial g_{\kappa\lambda}}{\partial q^\mu}\right). \tag{14}$$

For more general cases with nonzero angular momentum, see Ref. [11].

Equation (13) suggests that ''forces'' can arise as is expected from the term in which the nonvanishing Christoffel symbol is involved due to the intrinsic non-Euclidean metric $g_{\mu\nu}$ in the internal space. We next investigate the dynamical significance of those forces by specifying particular internal coordinates explicitly.

III. THREE-ATOM SYSTEM

We now work on the structural isomerization dynamics of three-atom clusters of zero angular momentum on the basis of the general formalism presented in the preceding section using the PAHC [17–20]. Although a three-atom cluster is obviously the simplest, it contains many of the general and essential features common to all other isomerization dynamics.

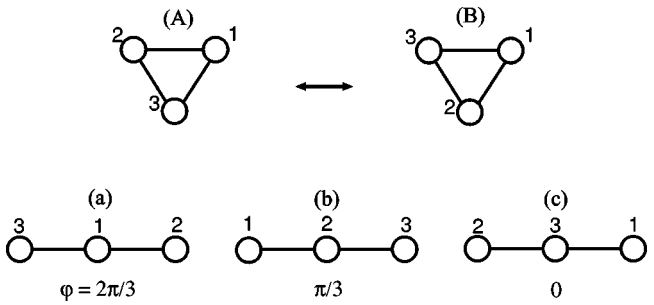

FIG. 1. Equilibrium and saddle structures of the three-atom Morse cluster. The equilibrium structure has two permutational isomers [(A) and (B)], while the saddle has three [(a), (b), and (c)]. The equilibrium structure is an equilateral triangle and the saddle structure is collinear. φ is the hyperangle defined in Eq. (21). Structural isomerization reaction occurs passing through the vicinity of one of the three saddle configurations. The potential energy of the equilibrium structure is -3.00ε and that of the saddle structure is -2.005ε.

A. Model system: M_3 cluster

The model system we study in this section is a cluster composed of three identical atoms (M_3 cluster), which mutually interact through the pairwise Morse potential. The total angular momentum is restricted to zero throughout. The Hamiltonian $\mathcal{H}/\varepsilon$ of this system has the following dimensionless form:

$$\frac{\mathcal{H}}{\varepsilon}=\frac{1}{2}\sum_{i=1}^{n}\left[\left(\frac{dr_{six}}{dt}\right)^2+\left(\frac{dr_{siy}}{dt}\right)^2+\left(\frac{dr_{siz}}{dt}\right)^2\right]+\sum_{i<j}\left[e^{-2(d_{ij}-d_0)}-2e^{-(d_{ij}-d_0)}\right], \tag{15}$$

where a set of coordinates $(r_{six},r_{siy},r_{siz})^T=\boldsymbol{r}_{si}$ represents the position of ith particle with respect to the space frame and ε represents the potential depth of Morse potential and d_{ij} is the interparticle distance between the ith and jth atoms. The particle number n is equal to three here. The parameter d_0, which corresponds to the equilibrium distance of the pairwise Morse potential, is only one parameter that controls the system dynamics. We set $d_0=6.0$ throughout this study, which provides a potential function similar to that of Lennard-Jones that is frequently used to model the van der Waals clusters. The masses of all particles can be set to unity. All the numerical results will thus be given in the absolute units. The molecule is laid on the x-y plane with $r_{s1z}=r_{s2z}=r_{s3z}=0$.

The M_3 cluster possesses two local equilibrium points at the potential energy $V=-3.00\varepsilon$ corresponding to the two permutationally distinctive equilateral triangle structures. It also has three saddle points that correspond to three permutationally distinctive collinear configurations whose potential energy is $V=-2.005\varepsilon$ (see Fig. 1). The isomerization reaction proceeds through the vicinity of these saddles.

B. The principal-axis hyperspherical coordinates and classical equations of motion

We begin with specifying the mass-weighted Jacobi vectors as

$$\boldsymbol{\rho}_{s1}=\sqrt{\mu_1}(\boldsymbol{r}_{s1}-\boldsymbol{r}_{s2}),\quad \mu_1=\frac{1}{2},$$

$$\boldsymbol{\rho}_{s2}=\sqrt{\mu_2}\left(\frac{\boldsymbol{r}_{s1}+\boldsymbol{r}_{s2}}{2}-\boldsymbol{r}_{s3}\right),\quad \mu_2=\frac{2}{3}, \tag{16}$$

where the vectors $\boldsymbol{\rho}_{si}$ $(i=1,2)$ and $\boldsymbol{r}_{si}$ $(i=1,2,3)$ are all three-dimensional vectors. Next, we define a 3×2 matrix W_s composed of the two Jacobi vectors

$$\mathsf{W}_s\equiv(\boldsymbol{\rho}_{s1}\ \boldsymbol{\rho}_{s2}). \tag{17}$$

According to the singular value decomposition theorem [31], the 3×2 matrix W_s is generally decomposed into the form

$$\mathsf{W}_s=\mathsf{RNU}^T=\begin{pmatrix}\boldsymbol{e}_1 & \boldsymbol{e}_2 & \boldsymbol{e}_3\end{pmatrix}\begin{pmatrix}a_1 & 0\\ 0 & a_2\\ 0 & 0\end{pmatrix}\begin{pmatrix}\boldsymbol{u}_1^T\\ \boldsymbol{u}_2^T\end{pmatrix}, \tag{18}$$

where R is a 3×3 orthogonal matrix, U is a 2×2 orthogonal matrix, and N is a 3×2 diagonal matrix whose diagonal elements a_1 and a_2 are called the singular values of W_s and the off-diagonal elements are all zero.

To specify the decomposition Eq. (18) more uniquely, we impose the following conditions on the matrices R, N, and U for our convenience. First, we set $a_1\geqslant|a_2|\geqslant0$, and let a_2 classify the permutational isomers of the three-atom cluster [22]. That is, if $\hat{\boldsymbol{z}}\cdot(\boldsymbol{\rho}_{s1}\times\boldsymbol{\rho}_{s2})>0$, which is the case for the structures of type (A) in Fig. 1, a_2 is positive. Otherwise [type (B) in Fig. 1], a_2 is negative, where $\hat{\boldsymbol{z}}$ is a unit vector along the positive z axis. The squares of the singular values, a_1^2 and a_2^2, are eigenvalues of a 3×3 matrix $\mathsf{W}_s\mathsf{W}_s^T$ and a 2×2 matrix $\mathsf{W}_s^T\mathsf{W}_s$ (the nonzero eigenvalues of $\mathsf{W}_s\mathsf{W}_s^T$ and $\mathsf{W}_s^T\mathsf{W}_s$ are the same [21]). The three column vectors of R, which are denoted by $\boldsymbol{e}_1,\boldsymbol{e}_2$, and $\boldsymbol{e}_3$, are the orthonormal eigenvectors of the 3×3 matrix $\mathsf{W}_s\mathsf{W}_s^T$, that is,

$$(\mathsf{W}_s\mathsf{W}_s^T)\boldsymbol{e}_\alpha=a_\alpha^2\boldsymbol{e}_\alpha\quad(\alpha=1,2,3). \tag{19}$$

Let a_3^2 be the zero eigenvalue of $\mathsf{W}_s\mathsf{W}_s^T$ with the corresponding eigenvector $\boldsymbol{e}_3=(0,0,1)^T=\hat{\boldsymbol{z}}$. This is possible since our three-atom system is planar in the x-y plane. (For the same reason, the z components of $\boldsymbol{e}_1$ and $\boldsymbol{e}_2$ are always zero.) Thus, the essential freedom of the matrix R is restricted to the left-upper 2×2 part [see Eq. (21) below]. Notice that the eigenvectors $\boldsymbol{e}_1$, $\boldsymbol{e}_2$, and $\boldsymbol{e}_3=(0,0,1)^T$ coincide with the principal axes of the instantaneous moment of inertia tensor of this system, since the nondiagonal elements of moment of inertia tensor (with respect to the space-fixed frame) coincide with those of the matrix $\mathsf{W}_s\mathsf{W}_s^T$ except for their sign. On the other hand, the two column vectors composing U (the row vectors of U^T), which are denoted by $\boldsymbol{u}_1$ and $\boldsymbol{u}_2$, are the orthonormal eigenvectors of the 2×2 matrix $\mathsf{W}_s^T\mathsf{W}_s$. That is,

$$(\mathsf{W}_s^T\mathsf{W}_s)\boldsymbol{u}_\beta=a_\beta^2\boldsymbol{u}_\beta\quad(\beta=1,2). \tag{20}$$

Parametrizing R and U with angles θ and φ, respectively, within a proper rotation matrix, we rewrite Eq. (18) explicitly as

$$\mathsf{W}_s = \begin{pmatrix} \cos\theta & -\sin\theta & 0 \\ \sin\theta & \cos\theta & 0 \\ 0 & 0 & 1 \end{pmatrix} \begin{pmatrix} a_1 & 0 \\ 0 & a_2 \\ 0 & 0 \end{pmatrix} \begin{pmatrix} \cos\varphi & \sin\varphi \\ -\sin\varphi & \cos\varphi \end{pmatrix}. \tag{21}$$

In the decomposition Eq. (21), the leftmost matrix R identifies the body frame. In other words, the body frame is the principal-axis frame in the PAHC. We call this gauge the principal-axis gauge. With this gauge, the components of the Jacobi vectors with respect to the body frame, $\boldsymbol{\rho}_1$ and $\boldsymbol{\rho}_2$, are expressed as [cf. Eq. (1)]

$$\begin{pmatrix} \boldsymbol{\rho}_1 & \boldsymbol{\rho}_2 \end{pmatrix} = \mathsf{N}\mathsf{U}^T = \begin{pmatrix} a_1\cos\varphi & a_1\sin\varphi \\ -a_2\sin\varphi & a_2\cos\varphi \\ 0 & 0 \end{pmatrix}. \tag{22}$$

Hence, the three variables a_1, a_2, and φ define the internal coordinates. φ is usually referred to as the hyperangle.

The singular values a_1 and a_2 are called gyration radii [17], which represent the mass-weighted length of the system along each principal axis. [Indeed they are related to the principal moment of inertia by a simple relation. See Eq. (23) below.] The gyration radii a_1 and a_2 are further parametrized in terms of the polar coordinates in the usual treatment [17,20]. In this study, however, we do not do so in view of their physical meaning. The angle θ specifies the orientation of the principal-axis frame of the three-body system with respect to the space-fixed frame and has nothing to do with the shape of the system. The continuous change of θ or the action of an SO(3) matrix to W_s from the left corresponds to the usual (external) rotation of the system. On the other hand, the continuous change of φ or the action of an SO(2) [or generally O(2)] matrix to W_s from the right generally changes the shape of system and is called the democracy transformation or the kinematic rotation. We call it ''democratic rotation.'' Figure 2 shows that the configuration of the three-atom cluster on a plane changes in a democratic manner along an orbit of democratic rotation from $\varphi=0$ to $\varphi=2\pi$ with a_1, a_2, and θ fixed in Eq. (21).

Democratic rotation in the internal space should be distinguished from that in the (translation-reduced) configuration space. While the latter is 2πperiodic as in Fig. 2, the former is π periodic [22]. This is related to the fact that the shape of the three-atom system itself distinguishing the permutations of atoms returns to the initial shape and only the spatial inversion (external rotation by π) occurs after a continuous democratic rotation in the configuration space by the angle π (See Fig. 2). This can be also seen by comparing the change in φ to $\varphi+\pi$ with fixing a_1, a_2, and θ in Eq. (21) and the change of θ to $\theta+\pi$ with fixing a_1, a_2, and φ. Thus the range of the hyperangle φ as an internal coordinate is set to $0\leqslant\varphi<\pi$.

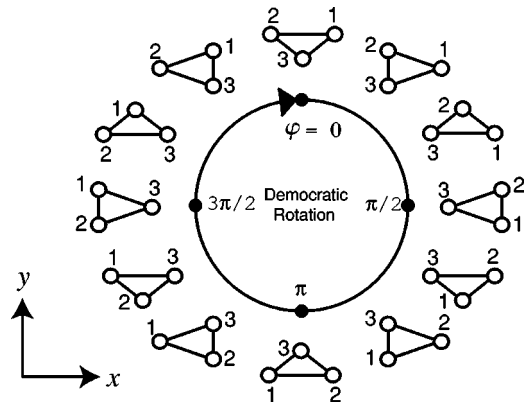

FIG. 2. A schematic figure of democratic (kinematic) rotation of a three-atom cluster in configuration space with θ and the gyration radii, a_1 and a_2 ($a_1>a_2$), fixed in Eq. (21). Democratic rotation in configuration space is 2π periodic, while the shape of the system itself distinguishing permutational isomers is π periodic. Correspondence between the value of hyperangle φ and molecular configuration depends on the definition of the Jacobi vectors in Eq. (16).

We next calculate the quantities required for the Lagrangian, Eq. (12), on the basis of these coordinates. The moment of inertia tensor, Eq. (6), referred to the body frame R is

$$\mathsf{M} = \begin{pmatrix} a_2^2 & 0 & 0 \\ 0 & a_1^2 & 0 \\ 0 & 0 & a_1^2+a_2^2 \end{pmatrix}, \tag{23}$$

which is a diagonal matrix as naturally required by the principal-axis frame. Using Eq. (23) and the components of Jacobi vectors $\boldsymbol{\rho}_1$ and $\boldsymbol{\rho}_2$ in Eq. (22), we find for the gauge potential Eq. (7) in the PAHC,

$$\boldsymbol{A}_{a_1}=\mathbf{0},\quad \boldsymbol{A}_{a_2}=\mathbf{0},\quad \boldsymbol{A}_{\varphi}=\begin{pmatrix} 0 \\ 0 \\ -\dfrac{2a_1a_2}{a_1^2+a_2^2} \end{pmatrix}. \tag{24}$$

The first and second components of all the gauge potentials are zero because the internal motion of three-body systems under zero angular momentum is restricted within the xy plane. The pseudometric tensor $h_{\mu\nu}$, which is defined by Eq. (9) is also diagonal as

$$(h_{\mu\nu}) = \begin{pmatrix} 1 & 0 & 0 \\ 0 & 1 & 0 \\ 0 & 0 & a_1^2+a_2^2 \end{pmatrix}. \tag{25}$$

Putting these quantities all together into Eq. (11), one obtains the gauge-invariant metric tensor in the internal space $g_{\mu\nu}$ as

$$(g_{\mu\nu})=\begin{pmatrix} 1 & 0 & 0 \\ 0 & 1 & 0 \\ 0 & 0 & \dfrac{(a_1^2-a_2^2)^2}{a_1^2+a_2^2} \end{pmatrix}. \tag{26}$$

As seen from Eq. (26), the two-dimensional space of gyration radii, a_1 and a_2, itself is Euclidean because $g_{a_1a_1}=g_{a_2a_2}=1$ and $g_{a_1a_2}=g_{a_2a_1}=0$. We call this (a_1,a_2) space the gyration space.

To see the intrinsic role of the gauge-invariant metric tensor $g_{\mu\nu}$ in Eq. (26), let us consider geodesics on the internal space. The Lagrangian for the geodesics is

$$\mathcal{L}=\frac{1}{2}g_{\mu\nu}\dot{q}^\mu\dot{q}^\nu=\frac{1}{2}\left[\dot{a}_1^2+\dot{a}_2^2+\frac{(a_1^2-a_2^2)^2}{a_1^2+a_2^2}\dot{\varphi}^2\right]. \tag{27}$$

Since the hyperangle φ is cyclic in Lagrangian Eq. (27), the corresponding conjugate momentum, democratic angular momentum,

$$L_{\mathrm{D}}\equiv\frac{\partial\mathcal{L}}{\partial\dot{\varphi}}=\frac{(a_1^2-a_2^2)^2}{a_1^2+a_2^2}\dot{\varphi} \tag{28}$$

becomes a constant of motion along the geodesics. Applying the Lagrangian Eq. (27) to the Euler-Lagrange equation, we obtain classical equations of motion for the geodesics as

$$\ddot{a}_1=\frac{a_1(a_1^2+3a_2^2)(a_1^2-a_2^2)}{(a_1^2+a_2^2)^2}\dot{\varphi}^2\equiv f_{\mathrm{DC},1}, \tag{29}$$

$$\ddot{a}_2=\frac{a_2(a_2^2+3a_1^2)(a_2^2-a_1^2)}{(a_1^2+a_2^2)^2}\dot{\varphi}^2\equiv f_{\mathrm{DC},2}, \tag{30}$$

and

$$\frac{d}{dt}\left[\frac{(a_1^2-a_2^2)^2}{a_1^2+a_2^2}\dot{\varphi}\right]=0. \tag{31}$$

Equation (31) merely tells that the democratic angular momentum is constant. On the other hand, Eqs. (29) and (30) indicate that a force in the gyration space (denoted hereafter as $f_{\mathrm{DC},1}$ and $f_{\mathrm{DC},2}$, respectively) arises from the democratic rotations. We call this force democratic centrifugal force (DCF) since it is proportional to the square of the democratic angular velocity $\dot{\varphi}$. A field of the DCF in the gyration space for a selected democratic angular velocity $\dot{\varphi}$ is depicted with arrows in Fig. 3. As seen in the field there, the DCF works so as to avoid the degeneracy of the two gyration radii near the line of degeneracy, $a_1=|a_2|$. Also, the arrows in Fig. 3 tend to align parallel to the a_1 axis for large a_1 with small $|a_2|$. To demonstrate the effects of the DCF directly, we show in Fig. 4 the projections of geodesics in the internal space onto the gyration space emanating from a point that is close to the a_1 axis. Each of them possesses different democratic angular momentum, Eq. (28), which is constant along each geodesic.

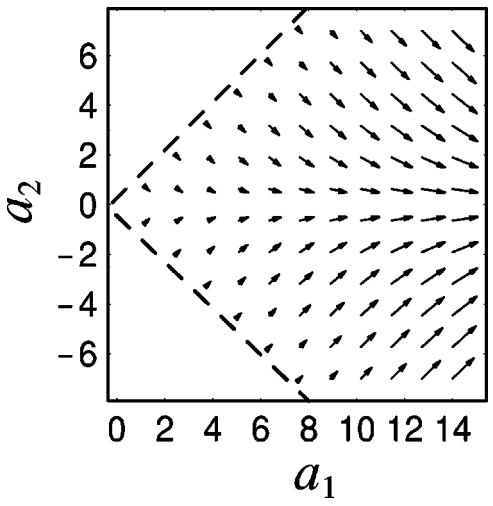

FIG. 3. Field of the democratic centrifugal force (DCF) on gyration space. Length of each arrow reflects the strength of the force at each point for a given value of democratic angular velocity $\dot{\varphi}$. The broken lines are the degeneracy lines between the two gyration radii, $a_1=|a_2|$. In four-atom clusters, a_1 and a_2 are replaced with a_α and a_β $(\alpha,\beta=1,2,3,\alpha\neq\beta,a_\alpha\geqslant a_\beta)$ respectively.

It has been thus confirmed that the geodesics are curved under the influence of the democratic centrifugal force.

Next, we set the equations of motion for the interacting three-body systems such as our three-atom clusters. The trivial change of the Lagrangian is

$$\mathcal{L}=\frac{1}{2}\left[\dot{a}_1^2+\dot{a}_2^2+\frac{(a_1^2-a_2^2)^2}{a_1^2+a_2^2}\dot{\varphi}^2\right]-V(a_1,a_2,\varphi). \tag{32}$$

Concomitantly, the classical equations of motion (for zero total angular momentum) are modified to

$$\ddot{a}_1=f_{\mathrm{DC},1}-\frac{\partial V}{\partial a_1}, \tag{33}$$

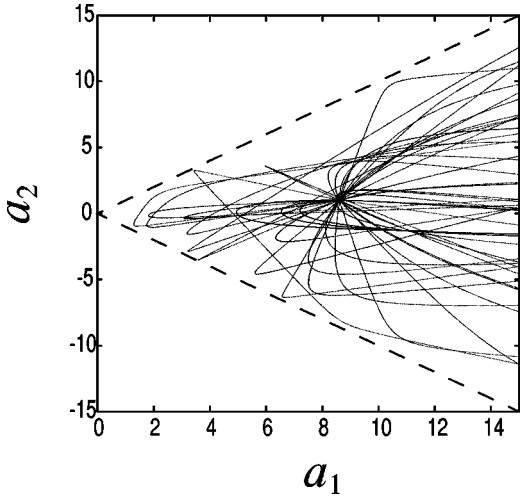

FIG. 4. Geodesics of the internal space projected onto the gyration space starting in the vicinity of a point $(a_1,a_2)=(8.6,1.0)$. Total energy of the three-atom system is $E=-1.37\varepsilon$ and total angular momentum of the system is zero. The broken lines are the degeneracy lines between the two gyration radii, $a_1=|a_2|$.

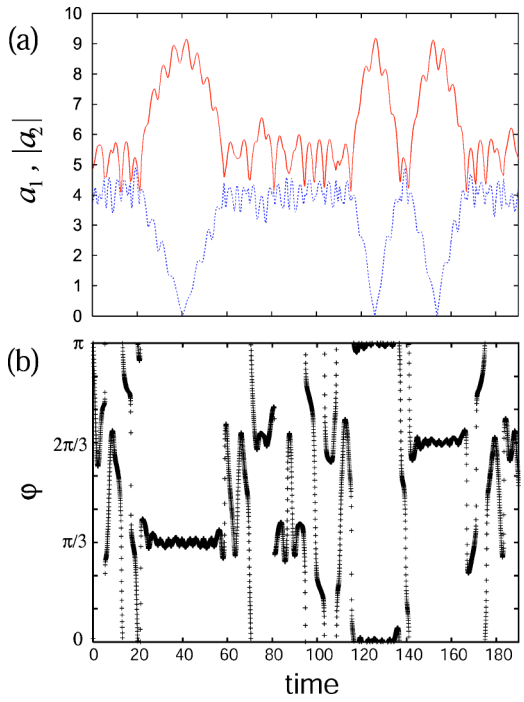

FIG. 5. (Color online) Typical time evolutions of the two gyration radii, a_1,$|a_2|$ ($a_1 \geqslant |a_2|$) and the hyperangle φ in the three-atom cluster at total energy $E=-1.53\varepsilon$. The condition $|a_2|=0$ represents the collinear configurations. The saddle crossing has taken place three times in this period. The locked angle $\varphi=0,\pi/3,2\pi/3$ specifies the three permutationally distinctive saddle configurations.

$$\ddot{a}_2 = f_{\mathrm{DC},2} - \frac{\partial V}{\partial a_2}, \tag{34}$$

$$\dot{L}_{\mathrm{D}} = -\frac{\partial V}{\partial \varphi}, \tag{35}$$

in abbreviated expressions. It is therefore expected that not only the usual potential force but also the democratic centrifugal force are responsible for the dynamics of the gyration radii. Indeed, we will see later that they mutually compete to dominate the collective motions of clusters.

C. Reaction path and the potential in the gyration space

We now study the structural isomerization dynamics of the M_3 cluster in terms of the PAHC presented above. First, the typical time evolutions of a_1, $|a_2|$, and φ, are depicted in Fig. 5. When the cluster geometry passes one of the collinear configurations, the smaller gyration radius a_2 becomes zero. The trajectory in Fig. 5(a) exhibits such barrier crossing three times. A remarkable fact found is that the hyperangle φ is practically ''locked'' at certain angles with a slight oscillation on the occasion of the isomerizing motions [compare the panels (a) and (b) in Fig. 5]. On the other hand, in the time interval of no reaction, φ varies very rapidly without such a locking. We have confirmed numerically that these behaviors are common to all the isomerization events of this M_3 cluster. Thus it turns out that the dynamics of the cluster has two qualitatively distinctive stages; one is the period of

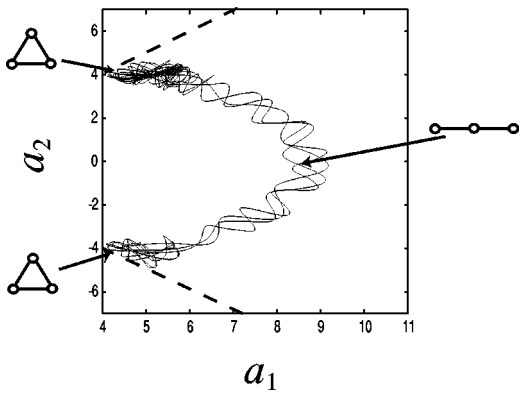

FIG. 6. A trajectory on the gyration space corresponding to the time evolution in Fig. 5. The permutationally distinctive equilibrium structures (equilateral triangles) are located at (4.24,4.24) and (4.24,−4.24), and the transition state (collinear) is located at (8.48,0). The broken lines indicate the degeneracy lines of $a_1=|a_2|$.

rapid democratic rotations during which the absolute values of the two gyration radii are close to each other, reflecting the fact that the shape of the cluster is close to the equilateral triangle, while the other is the period of hyperangle locking during which collective isomerizing motions occur.

The locking of φ on the occasion of barrier crossing contains important pieces of information about the reaction channel. We observe in Fig. 5 that φ is locked around 0, $\pi/3$, or $2\pi/3$. (Note that $\varphi=0$ and $\varphi=\pi$ are connected since φ is π periodic.) Substituting $\varphi=0$, $\pi/3$, and $2\pi/3$ into Eq. (22), we see that these angles of φ specify three permutationally distinctive oblate-isosceles-triangle structures of the cluster. This can also be seen in Fig. 2. For an extreme instance, $a_2=0$ with $\varphi=0$, $\pi/3$, or $2\pi/3$, gives rise to a respective collinear geometry in which the central atom is located at the centroid (see Fig. 1). Hence, isomerization with the hyperangle locked around 0, $\pi/3$, or $2\pi/3$ implies that the isomerization reaction proceeds mostly keeping the isosceles-triangle configurations.

The mechanism of locking of the hyperangle in the isomerization reaction can be understood phenomenologically as follows. We first map the trajectory of Fig. 5 onto the gyration space as in Fig. 6. In the gyration space, the two permutationally distinctive local equilibrium structures (equilateral triangles) are located at (4.24,4.24) and (4.24, −4.24), and the collinear transition state is located at (8.48,0). From the trajectory in Fig. 6, a rough picture of the reaction path can be readily obtained. We now plot the potential-energy surface in the gyration space as a function of the hyperangle. Figure 7(a) depicts contours of $V(a_1,a_2,\varphi)$ with φ fixed at 0, $\pi/3$, or $2\pi/3$. The topography of them for these three angles is exactly the same. We observe that the two potential basins in Fig. 7(a) are connected by a saddle at a reasonably low energy, which allows the isomerization. However, a slightly different hyperangle deforms the contours of $V(a_1,a_2,\varphi)$ dramatically as shown in Figs. 7(b) and 7(c), where φ is displaced only by $\pi/30$ and $\pi/12$, respectively. It turns out that the height of potential barrier along the reaction path increases drastically if φ is

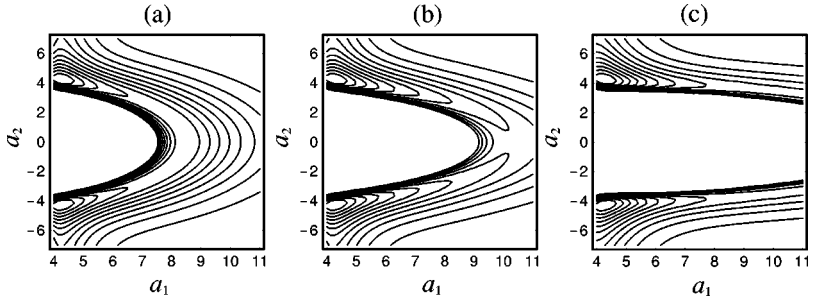

FIG. 7. Potential-energy surfaces $V(a_1,a_2,\varphi)$ in the gyration space. The hyperangle is fixed to (a) $\varphi=0$, or $\pi/3$, or $2\pi/3$, (b) $\varphi=(0,\pi/3,$ or $2\pi/3)+\pi/30$, and (c) $\varphi=(0,\pi/3,$ or $2\pi/3)+\pi/12$. The potential energy at $(a_1,a_2)=(4.24, \pm 4.24)$ is -3.00ε in all the three parts. The energy difference between two neighboring contour lines is 0.231ε.

shifted away from 0, $\pi/3$, or $2\pi/3$ and the reaction path is immediately closed. This explains why the gyration radii a_1 and $|a_2|$ are mostly localized in the vicinity of their equilibrium values (≈ 4.24) before an isomerization begins (See Fig. 5), and also why the isomerization is virtually impossible unless the hyperangle φ is close to 0, $\pi/3$, or $2\pi/3$. Thus, the gate opening of the reaction path is controlled in φ.

On the other hand, the stability of the locking of φ around the collinear configuration is explained as follows. Figure 8 shows the potential profiles along φ for four given sets of gyration radii, $(a_1,a_2)=(4.24,4.24)$, (5.0,3.9), (6.0,3.5), and (8.48,0). These points have been picked up from the reaction coordinate of Fig. 7(a). The potential curve against φ is flatter for the values of gyration radii closer to their equilibrium values, $(a_1,|a_2|)=(4.24,4.24)$, allowing a rapid democratic rotation around the equilibrium points. On the other hand, the profile corresponding to the saddle point $(a_1,a_2)=(8.48,0)$ has a very deep valley in the vicinity of $\varphi=0$, $\pi/3$, and $2\pi/3$. Thus only a very narrow range in φ is energetically accessible in passing through the saddle region for the present isomerization dynamics. We will discuss a trapped motion arising from this locking phenomenon later in a greater detail.

Based on the above observations, the reaction mechanism of M_3 cluster can be summarized as follows. In the motions around the local equilibrium structure, a trajectory in the gyration space searches for a chance to get into the entrance of the reaction channel. The gate to that channel is opened and closed frequently by the rapid democratic rotations. In this regime, the dynamics of the cluster is dominated by all

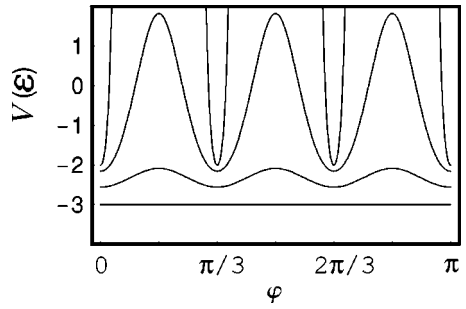

FIG. 8. Potential-energy curves against the hyperangle φ with gyration radii a_1 and a_2 fixed to $(a_1,a_2)=(4.24,4.24),(5.0,3.9),(6.0,3.5),(8.48,0)$ from the bottom to the top. These values are selected along the reaction coordinate in Fig. 7(a).

of a_1, a_2, and φ. Once a trajectory successfully gets into the reaction pathway, the hyperangle is locked around the certain values, which leads to a collective motion in a_1 and a_2.

D. Role of the democratic centrifugal force: Inducing mass-balance asymmetry

In the above presented reaction mechanism, the role of the DCF, which is expected to affect the behavior in the gyration space as suggested in Eq. (33) and Eq. (34), is quite interesting. According to the field of the DCF in the gyration space (see Fig. 3), the DCF is generally expected to distort the M_3 cluster into a collapsed structure, since it tends to increase a_1 and decrease $|a_2|$. With this fundamental feature in mind, we explore the effects of the DCF on the dynamics of M_3 in this and next subsections. We first study the dynamics around the equilibrium structures.

At first glance at the definition of DCF in Eq. (29) and Eq. (30) or the field of DCF in Fig. 3, one might think that the DCF must be small near the line of degeneracy, namely, $a_1=|a_2|$. However, this is not the case since the $\dot{\varphi}$ dependence of the DCF is not taken into this consideration. (Recall that Fig. 3 shows a field of DCF for a fixed value of $\dot{\varphi}$.) In fact, as we have actually seen in Fig. 5, very rapid democratic rotation takes place in the vicinity of the local equilibrium structure, at which the two gyration radii are close to each other $a_1\approx|a_2|$. [Compare the panels (a) and (b) in Fig. 5.] This situation is understood by expressing $\dot{\varphi}$ explicitly as

$$\dot{\varphi}=\dot{\boldsymbol{u}}_1\cdot\boldsymbol{u}_2=\frac{\boldsymbol{u}_1^T(\dot{\mathsf{W}}_s^T\mathsf{W}_s+\mathsf{W}_s^T\dot{\mathsf{W}}_s)\boldsymbol{u}_2}{a_1^2-a_2^2}, \tag{36}$$

which is obtained by differentiating Eq. (20) with respect to time. Since the numerator of Eq. (36) is generally not zero, $a_1\approx|a_2|$ should lead to a very large $\dot{\varphi}$, which in turn implies very rapid democratic rotation.

Substituting Eq. (36) into the expressions for the DCF defined in Eq. (29) and Eq. (30), we obtain

$$f_{\mathrm{DC},1}=\frac{a_1(a_1^2+3a_2^2)}{(a_1^2+a_2^2)^2}\,\frac{[\boldsymbol{u}_1^T(\dot{\mathsf{W}}_s^T\mathsf{W}_s+\mathsf{W}_s^T\dot{\mathsf{W}}_s)\boldsymbol{u}_2]^2}{a_1^2-a_2^2}, \tag{37}$$

$$f_{\mathrm{DC},2}=\frac{a_2(a_2^2+3a_1^2)}{(a_1^2+a_2^2)^2}\,\frac{[\boldsymbol{u}_1^T(\dot{\mathsf{W}}_s^T\mathsf{W}_s+\mathsf{W}_s^T\dot{\mathsf{W}}_s)\boldsymbol{u}_2]^2}{a_2^2-a_1^2}, \tag{38}$$

both of which again diverge to infinity at $a_1=|a_2|$ on gyration space. Thus, the rapid democratic rotation near the de-

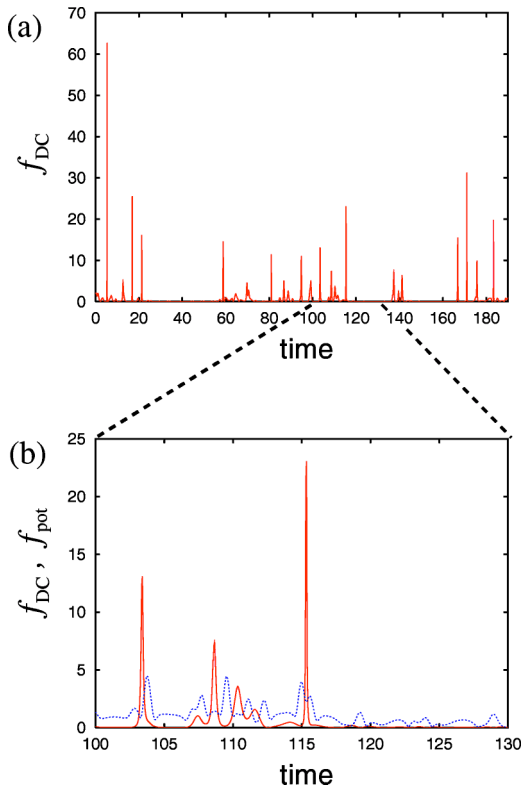

FIG. 9. (Color online) (a) Time evolution of the absolute value of the democratic centrifugal force, $f_{DC}=\sqrt{f_{DC,1}^2+f_{DC,2}^2}$ (solid line) along the same trajectory as in Fig. 5. (b) A magnified view of (a), where the time evolution of the absolute value of the potential force, $f_{pot}=\sqrt{(\partial V/\partial a_1)^2+(\partial V/\partial a_2)^2}$ (broken line), is also displayed for comparison.

generacy line, $a_1=|a_2|$, can generate a very strong DCF. Figure 9(a) exemplifies a time evolution of $f_{DC}=\sqrt{f_{DC,1}^2+f_{DC,2}^2}$ along the trajectory of Figure 5. Fig. 9(b) magnifies the scale of Fig. 9(a), in which the force arising from the potential energy $f_{pot}=\sqrt{(\partial V/\partial a_1)^2+(\partial V/\partial a_2)^2}$ is plotted together for comparison. In Fig. 9, f_{DC} often appears as a δ-function-like peak in response to the rapid democratic rotations. (Compare Fig. 9 with Fig. 5.) Figure 9 suggests that the DCF is well comparable with the potential force in magnitude. What is more, the DCF is much stronger than the potential force near the degeneracy line at $a_1\approx|a_2|$.

Thus, the dynamics near the equilateral triangle structure is strongly influenced by the DCF. In fact, we see from Fig. 6 that the trajectory in the gyration space is strongly repulsed from the line of degeneracy, $a_1=|a_2|$. That is, $a_1=|a_2|$ tends to be avoided so that the mass-balance deviates from that of the equilateral triangle structure. In this way, the DCF helps trajectories to get into the reaction pathway.

E. Role of the democratic centrifugal force: Trapping the trajectories around the transition state

The effect of the DCF becomes more prominent in the vicinity of the transition state. When the trajectories undergo reaction with the hyperangle φ being locked around 0, $\pi/3$, or $2\pi/3$, φ generally oscillates within a small range around these angles. This in turn gives birth to the DCF, which is as significant as the potential force in the present system. The DCF thus generated in the configuration around the transition state (collinear geometry) induces a trapped motion of trajectories: The M_3 cluster often shows a peculiar behavior to recross the collinear structure many times before falling down to the bottom region of the potential basin. A typical time evolution of the gyration radii for that kind of motion is shown in Fig. 10. In this figure, the gyration radii a_1 and a_2 keep close to the values of the collinear saddle structure for a long time before going to the vicinity of their equilibrium value ($a_1=|a_2|=4.24$), which clearly demonstrates the trapped and recrossing motion around the collinear structure.

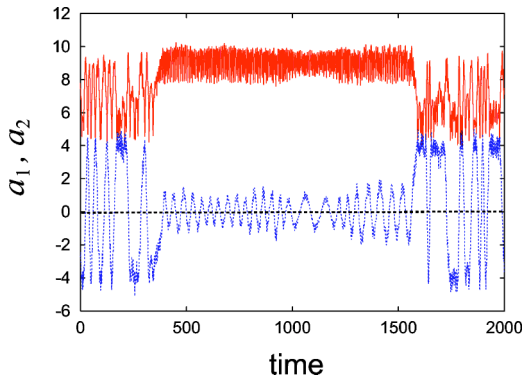

FIG. 10. (Color online) A typical time evolution of the gyration radii, a_1 and a_2 ($a_1\geqslant a_2$), which shows a trapped motion in the vicinity of the collinear saddle structure from $t\approx 400$ to $t\approx 1600$, recrossing the dividing surface many times. Total internal energy of the trajectory is $E=-1.17\varepsilon$.

It is not trivial for this trapped motion to take place in such a saddle region. This phenomenon can be physically rationalized as follows. As we have seen in Fig. 3, DCF generally arises in the direction that makes the gyration radius a_1 larger and $|a_2|$ smaller (recall we defined $a_1\geqslant|a_2|$). This general characteristic tends to push a trajectory in the gyration space toward the line, $|a_2|=0$, which corresponds to the collinear structures. This force applies from both basins, preventing the trajectory from falling down to the valley regions. To make this point clearer, let us regroup the Lagrangian of Eq. (32) as

$$\mathcal{L}=\frac{1}{2}[\dot{a}_1^2+\dot{a}_2^2]-\left[V(a_1,a_2,\varphi)-\frac{1}{2}\frac{(a_1^2-a_2^2)^2}{a_1^2+a_2^2}\dot{\varphi}^2\right], \tag{39}$$

with which the dynamics in (a_1,a_2) space under a given φ and $\dot{\varphi}$ is represented. We thus see an effective potential as

$$V_{\text{eff}}=-\frac{1}{2}\frac{(a_1^2-a_2^2)^2}{a_1^2+a_2^2}\dot{\varphi}^2+V(a_1,a_2,\varphi). \tag{40}$$

Figure 11 exemplifies such an effective potential-energy surface for $\varphi=0$ (or $\pi/3$, or $2\pi/3$) with $|\dot{\varphi}|=0.05$, which is a roughly averaged value during the period of the trapped motions. The figure exhibits a basin that newly appears at the

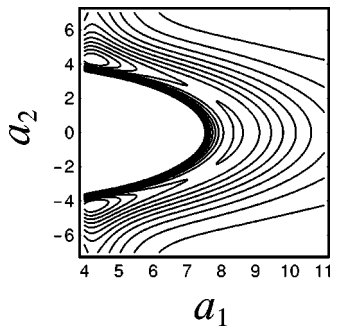

FIG. 11. Effective potential-energy surface, Eq. (40), on the gyration space fixing the hyperangle φ to 0, $\pi/3$, or $2\pi/3$. The democratic angular velocity is set to $|\dot{\varphi}|=0.05$. The energy difference between two neighboring contour lines is 0.231ε.

former saddle point. With increasing $\dot{\varphi}$, the present basin becomes wider and deeper in general. The trapped motion is thus rationalized from the view point of energetics, too.

In chemical reaction dynamics of three atomic exchange reaction such as the $H+H_2$ reaction, recrossing over a dividing surface at the transition state has been studied within the scheme of collinear configuration [28,29]. The existence of a resonance on the skewed potential surface yields bouncing motions in the transition-state region. The trapped motion we have discussed above is different from this well-established one. As seen in Fig. 11, the trapped motion is basically supported by the effective local minimum on the transition state, which allows the oscillations not only within the collinear configuration (along a_1) but in the direction of the bending-like motion out of collinear configuration (along a_2).

The above argument leading to Fig. 11 also sheds light on the dynamical regularity in the dynamics around the saddle region. Berry and co-workers [3–5] have found and discussed that dynamics and related phase-space structure around the transition state is more stable than is expected as a theoretical foundation of the statistical chemical reaction theories like the transition-state theory. There are two major points to account for this phenomenon from our point of view. First, the effective degrees of freedom that dominate the collective motion in crossing the saddle region are reduced (from three to two in the present case) due to the hyperangle locking. As shown in Fig. 5 through Fig. 7, the collective motion was essentially dominated by the two parameters, a_1 and a_2. Second, the regularity of the saddle crossing motions is brought about by the existence of the new basin in the transition-state region (Fig. 11).

IV. FOUR-ATOM SYSTEM

We proceed to the structural isomerization dynamics of a Morse cluster composed of four identical atoms, M_4. The total angular momentum is again zero. The basic strategy of our analysis here is similar to that of three-atom systems studied in the preceding section. The main difference is that the gyration space in six-dimensional internal space becomes three dimensional. Nevertheless, it is shown that only two gyration radii out of six independent variables can be regarded essentially as collective coordinates that dominate the isomerization reaction.

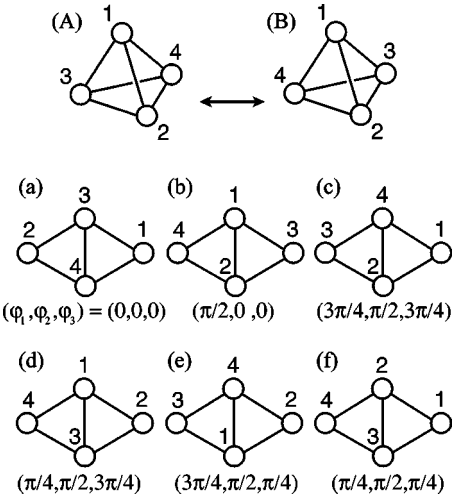

FIG. 12. Local equilibrium and saddle structures of a four-atom Morse cluster. The local equilibrium structures (tetrahedral structures) and the first rank saddle structures (planar rhombus-shaped structures) have the energies -6.00ε and -5.02ε, respectively. φ_1, φ_2, and φ_3 are the hyperangles. When $\varphi_2=0$, φ_1 and φ_3 cannot be determined uniquely and only the summation $\varphi_1+\varphi_3$ is meaningful due to the convention for Euler angles in Eq. (45). Hence, we set $\varphi_3=0$ when $\varphi_2=0$.

A. Model system: M_4 cluster

The Hamiltonian of the system in this section is similar to Eq. (15) except that $n=4$. Local equilibrium structures of this cluster are tetrahedral, having the potential energy -6.0ε. There exist two permutationally distinctive isomers as shown in Fig. 12. The first rank saddle point on the potential-energy surface corresponds to the planar rhombus-shaped structure, whose potential energy is -5.02ε. (The square planar structure is a second-rank saddle.) There are six permutationally distinctive saddles on the potential surfaces which are also depicted in Fig. 12. Structural isomerization proceeds through these saddle structures.

B. PAHC and classical equations of motion

We now introduce the principal-axis hyperspherical coordinates for the four-atom systems extending the methods for the three-atom systems in the preceding section. First, we define mass-weighted Jacobi vectors as

$$\boldsymbol{\rho}_{s1}=\sqrt{\mu_1}(\boldsymbol{r}_{s1}-\boldsymbol{r}_{s2}),\quad \mu_1=\frac{1}{2},$$

$$\boldsymbol{\rho}_{s2}=\sqrt{\mu_2}(\boldsymbol{r}_{s3}-\boldsymbol{r}_{s4}),\quad \mu_2=\frac{1}{2}, \tag{41}$$

$$\boldsymbol{\rho}_{s3}=\sqrt{\mu_3}\left(\frac{\boldsymbol{r}_{s1}+\boldsymbol{r}_{s2}}{2}-\frac{\boldsymbol{r}_{s3}+\boldsymbol{r}_{s4}}{2}\right),\quad \mu_3=1.$$

This choice results that reaction channels are specified by multiples of $\pi/4$ in the hyperangles.

The 3×3 matrix W_s whose columns are the three mass-weighted Jacobi vectors is decomposed as

$$\mathsf{W}_s\equiv\begin{pmatrix}\boldsymbol{\rho}_{s1} & \boldsymbol{\rho}_{s2} & \boldsymbol{\rho}_{s3}\end{pmatrix}=\mathsf{R}\mathsf{N}\mathsf{U}^T\equiv\begin{pmatrix}\boldsymbol{e}_1 & \boldsymbol{e}_2 & \boldsymbol{e}_3\end{pmatrix}\times\begin{pmatrix}a_1 & 0 & 0\\ 0 & a_2 & 0\\ 0 & 0 & a_3\end{pmatrix}\begin{pmatrix}\boldsymbol{u}_1^T\\ \boldsymbol{u}_2^T\\ \boldsymbol{u}_3^T\end{pmatrix}, \tag{42}$$

where both matrices R and U belong to SO(3). The unit vectors $\{\boldsymbol{e}_\alpha\}$ and $\{\boldsymbol{u}_\beta\}$ $(\alpha,\beta=1,2,3)$, and the singular values a_1,a_2, and a_3 are solutions of the eigenvalue problems,

$$(\mathsf{W}_s\mathsf{W}_s^T)\boldsymbol{e}_\alpha=a_\alpha^2\boldsymbol{e}_\alpha\quad(\alpha=1,2,3), \tag{43}$$

$$(\mathsf{W}_s^T\mathsf{W}_s)\boldsymbol{u}_\beta=a_\beta^2\boldsymbol{u}_\beta\quad(\beta=1,2,3). \tag{44}$$

We define the order of the singular values as $a_1\geqslant a_2\geqslant|a_3|$. The planar and collinear configurations give $a_3=0$ and $a_2=a_3=0$, respectively. Furthermore, we let the sign of a_3 specify the permutational isomers of the cluster [23]. That is, if $(\det\mathsf{W}_s)=\boldsymbol{\rho}_{s1}\cdot(\boldsymbol{\rho}_{s2}\times\boldsymbol{\rho}_{s3})\geqslant0$, which is the case for isomer (A) in Fig. 12, $a_3\geqslant0$. Otherwise, $a_3<0$. Eigenvectors $\boldsymbol{e}_\alpha$ $(\alpha=1,2,3)$ coincide with the principal axes of instantaneous moment of inertia tensor. We thereby refer to the principal-axis frame as a body frame. On the other hand, the triplet of axes $(\boldsymbol{u}_1,\boldsymbol{u}_2,\boldsymbol{u}_3)$ or an SO(3) matrix U constitutes a democracy frame. The democracy frame rotates in a three-dimensional space and is parametrized by the usual Euler angles $(\varphi_1,\varphi_2,\varphi_3)$ as [32]

$$\mathsf{U}^T=\begin{pmatrix}\cos\varphi_1\cos\varphi_3-\sin\varphi_1\cos\varphi_2\sin\varphi_3 & \cos\varphi_1\sin\varphi_3-\sin\varphi_1\cos\varphi_2\cos\varphi_3 & \sin\varphi_1\sin\varphi_2\\ -\sin\varphi_1\cos\varphi_3-\cos\varphi_1\cos\varphi_2\sin\varphi_3 & -\sin\varphi_1\sin\varphi_3+\cos\varphi_1\cos\varphi_2\cos\varphi_3 & \cos\varphi_1\sin\varphi_2\\ \sin\varphi_2\sin\varphi_3 & -\sin\varphi_2\cos\varphi_3 & \cos\varphi_2\end{pmatrix}. \tag{45}$$

The angular velocity of democracy frame with respect to the democracy frame itself, $\boldsymbol{\gamma}_{\mathrm{D}}$, is expressed in the usual manner [32] using the Euler angles and their time-derivatives as

$$\boldsymbol{\gamma}_{\mathrm{D}}\equiv\begin{pmatrix}\gamma_{23}\\ \gamma_{31}\\ \gamma_{12}\end{pmatrix}=\begin{pmatrix}0 & \cos\varphi_1 & \sin\varphi_1\sin\varphi_2\\ 0 & -\sin\varphi_1 & \cos\varphi_1\sin\varphi_2\\ 1 & 0 & \cos\varphi_2\end{pmatrix}\begin{pmatrix}\dot{\varphi}_1\\ \dot{\varphi}_2\\ \dot{\varphi}_3\end{pmatrix}, \tag{46}$$

where we have defined the components of $\boldsymbol{\gamma}_{\mathrm{D}}$ as $\gamma_{\alpha\beta}=\dot{\boldsymbol{u}}_\alpha\cdot\boldsymbol{u}_\beta$ $(\alpha,\beta=1,2,3,\alpha\neq\beta)$, which represents the strength of coupling between the αth and βth axes in the democracy frame. The components $\gamma_{\alpha\beta}$ are antisymmetric with respect to the exchange of α and β, namely, $\gamma_{\alpha\beta}=-\gamma_{\beta\alpha}$. We also define the 3×3 matrix in the right-hand side of Eq. (46) as Λ. It can be proved [20,23] that the ranges of the hyperangles in the internal space $(a_1,a_2,a_3,\varphi_1,\varphi_2,\varphi_3)$ are restricted to

$$0\leqslant\varphi_1,\varphi_3<\pi,\quad 0\leqslant\varphi_2\leqslant\pi. \tag{47}$$

Next, we construct the Lagrangian for the zero-angular-momentum case. The moment of inertia tensor M in Eq. (6) is diagonal as

$$\mathsf{M}=\begin{pmatrix}a_2^2+a_3^2 & 0 & 0\\ 0 & a_3^2+a_1^2 & 0\\ 0 & 0 & a_1^2+a_2^2\end{pmatrix}, \tag{48}$$

since we refer to the principal-axis frame R. The gauge potential in our principal-axis gauge is obtained by invoking Eq. (7). The result for the gyration radii a_1,a_2, and a_3 is

$$\boldsymbol{A}_{a_1}=\boldsymbol{A}_{a_2}=\boldsymbol{A}_{a_3}=\boldsymbol{0}, \tag{49}$$

which is similar to the result of Eq. (24). On the other hand, the components of the gauge potential for the hyperangles φ_1,φ_2, and φ_3 are expressed collectively in a 3×3 matrix form as

$$\begin{pmatrix}\boldsymbol{A}_{\varphi_1} & \boldsymbol{A}_{\varphi_2} & \boldsymbol{A}_{\varphi_3}\end{pmatrix}=\mathsf{M}^{-1}\mathsf{b}\Lambda, \tag{50}$$

where a 3×3 diagonal matrix b is defined as

$$\mathsf{b}\equiv\begin{pmatrix}-2a_2a_3 & 0 & 0\\ 0 & -2a_3a_1 & 0\\ 0 & 0 & -2a_1a_2\end{pmatrix}, \tag{51}$$

and Λ is the 3×3 matrix defined in Eq. (46).

The pseudometric tensor $h_{\mu\nu}$ in Eq. (9) for the internal coordinates $(a_1,a_2,a_3,\varphi_1,\varphi_2,\varphi_3)$ becomes

$$(h_{\mu\nu})=\begin{pmatrix}\mathsf{I} & \mathsf{0}\\ \mathsf{0} & \Lambda^T\mathsf{M}\Lambda\end{pmatrix}, \tag{52}$$

where I is a 3×3 unit matrix. The components of the matrix are ordered in accordance with that of $(a_1,a_2,a_3,\varphi_1,\varphi_2,\varphi_3)$. For example, the (3,4) component

of $(h_{\mu\nu})$ is $h_{a_3\varphi_1}$. Putting Eqs. (48), (49), (50), and (52) into Eq. (11) we obtain the gauge-invariant metric tensor of internal space as

$$(g_{\mu\nu})=\begin{pmatrix} \mathsf{I} & \mathsf{0} \\ \mathsf{0} & \Lambda^T(\mathsf{M}-\mathsf{b}\mathsf{M}^{-1}\mathsf{b})\Lambda \end{pmatrix}=\begin{pmatrix} \mathsf{I} & \mathsf{0} \\ \mathsf{0} & \Lambda^T\tilde{\mathsf{M}}\Lambda \end{pmatrix}, \tag{53}$$

where the diagonal matrix $\tilde{\mathsf{M}}$ is defined as

$$\tilde{\mathsf{M}}\equiv\mathsf{M}-\mathsf{b}\mathsf{M}^{-1}\mathsf{b}=\begin{pmatrix} \dfrac{(a_2^2-a_3^2)^2}{a_2^2+a_3^2} & 0 & 0 \\ 0 & \dfrac{(a_3^2-a_1^2)^2}{a_3^2+a_1^2} & 0 \\ 0 & 0 & \dfrac{(a_1^2-a_2^2)^2}{a_1^2+a_2^2} \end{pmatrix}. \tag{54}$$

In terms of the vectors $\boldsymbol{a}=(a_1,a_2,a_3)^T$ and $\boldsymbol{\varphi}=(\varphi_1,\varphi_2,\varphi_3)^T$, the kinetic energy K with zero angular momentum is represented with use of Eq. (53) as

$$2K=(\dot{\boldsymbol{a}}^T\ \dot{\boldsymbol{\varphi}}^T)\begin{pmatrix} \mathsf{I} & \mathsf{0} \\ \mathsf{0} & \Lambda^T\tilde{\mathsf{M}}\Lambda \end{pmatrix}\begin{pmatrix} \dot{\boldsymbol{a}} \\ \dot{\boldsymbol{\varphi}} \end{pmatrix}=(\dot{\boldsymbol{a}}^T\ \boldsymbol{\gamma}_{\mathrm{D}}^T)\begin{pmatrix} \mathsf{I} & \mathsf{0} \\ \mathsf{0} & \tilde{\mathsf{M}} \end{pmatrix}\begin{pmatrix} \dot{\boldsymbol{a}} \\ \boldsymbol{\gamma}_{\mathrm{D}} \end{pmatrix}, \tag{55}$$

where we have used the democratic angular velocity defined in Eq. (46) in the second equality. Thus, the Lagrangian is obtained as

$$\begin{aligned}\mathcal{L}=&\frac{1}{2}\dot{\boldsymbol{a}}^2+\frac{1}{2}\boldsymbol{\gamma}_{\mathrm{D}}^T\tilde{\mathsf{M}}\boldsymbol{\gamma}_{\mathrm{D}}-V(\boldsymbol{a},\boldsymbol{\varphi})=\frac{1}{2}(\dot{a}_1^2+\dot{a}_2^2+\dot{a}_3^2)\\&+\frac{(a_1^2-a_2^2)^2}{2(a_1^2+a_2^2)}\gamma_{12}^2+\frac{(a_2^2-a_3^2)^2}{2(a_2^2+a_3^2)}\gamma_{23}^2+\frac{(a_3^2-a_1^2)^2}{2(a_3^2+a_1^2)}\gamma_{31}^2\\&-V(a_1,a_2,a_3,\varphi_1,\varphi_2,\varphi_3).\end{aligned} \tag{56}$$

Classical equations of motion are then derived, the gyration components of which are

$$\ddot{a}_1=\frac{a_1(a_1^2+3a_2^2)(a_1^2-a_2^2)}{(a_1^2+a_2^2)^2}\gamma_{12}^2+\frac{a_1(a_1^2+3a_3^2)(a_1^2-a_3^2)}{(a_1^2+a_3^2)^2}\gamma_{13}^2-\frac{\partial V}{\partial a_1}, \tag{57}$$

$$\ddot{a}_2=\frac{a_2(a_2^2+3a_1^2)(a_2^2-a_1^2)}{(a_2^2+a_1^2)^2}\gamma_{21}^2+\frac{a_2(a_2^2+3a_3^2)(a_2^2-a_3^2)}{(a_2^2+a_3^2)^2}\gamma_{23}^2-\frac{\partial V}{\partial a_2}, \tag{58}$$

$$\ddot{a}_3=\frac{a_3(a_3^2+3a_2^2)(a_3^2-a_2^2)}{(a_3^2+a_2^2)^2}\gamma_{32}^2+\frac{a_3(a_3^2+3a_1^2)(a_3^2-a_1^2)}{(a_3^2+a_1^2)^2}\gamma_{31}^2-\frac{\partial V}{\partial a_3}, \tag{59}$$

and for the hyperangle part, based on the *vielbein* formalism [11], we have

$$\frac{d}{dt}(\tilde{\mathsf{M}}\boldsymbol{\gamma}_{\mathrm{D}})+\boldsymbol{\gamma}_{\mathrm{D}}\times(\tilde{\mathsf{M}}\boldsymbol{\gamma}_{\mathrm{D}})=-(\Lambda^{-1})^T\begin{pmatrix} \partial V/\partial\varphi_1 \\ \partial V/\partial\varphi_2 \\ \partial V/\partial\varphi_3 \end{pmatrix}. \tag{60}$$

In a system free of the potential term, the following democratic angular momentum vector:

$$\boldsymbol{L}_{\mathrm{D}}\equiv\mathsf{U}\tilde{\mathsf{M}}\boldsymbol{\gamma}_{\mathrm{D}} \tag{61}$$

becomes a constant of motion.

Similarly to the three-body systems, the democratic centrifugal force arises in the gyration space as is evident from the first and the second terms on the right-hand sides of Eqs. (57)–(59). Coupling between α axis and β axis $(\alpha,\beta=1,2,3, \alpha\neq\beta)$ of the democracy frame, which is characterized by $\gamma_{\alpha\beta}=\dot{\boldsymbol{u}}_\alpha\cdot\boldsymbol{u}_\beta$, yields the field of democratic centrifugal force on all the planes parallel to the a_α-a_β plane in the gyration space. Appearance of this field is exactly the same as that in Fig. 3, where a_1 and a_2 in Fig. 3 are replaced by a_α and a_β $(a_\alpha\geqslant a_\beta)$, respectively. Each term of the democratic centrifugal force is, again, proportional to the square of the components of the democratic angular velocity, $\gamma_{\alpha\beta}^2$. Along the a_1 axis of the gyration space, the democratic centrifugal force works always in the positive direction since $a_1^2-a_2^2\geqslant 0$ and $a_1^2-a_3^2\geqslant 0$ in Eq. (57). While, along the a_2 axis, it can work in both positive and negative directions depending on the sum of the first term (always negative) and the second term (always positive) on the right-hand side of Eq. (58). Finally, along the a_3 axis, it always works in the direction that the absolute value of a_3 is diminished since $a_3^2-a_2^2\leqslant 0$ and $a_3^2-a_1^2\leqslant 0$ in Eq. (59). Thus the four-atom cluster generally tends to be distorted in such a direction that massive directions should become more massive.

C. Reaction path in the gyration space

As we did in the case of three-atom clusters, we begin by searching the reaction paths for the four-atom cluster. In Fig. 13, we show a typical time evolution of gyration radii, a_1, a_2, and a_3, and hyperangles, φ_1, φ_2, and φ_3. When the values of the three gyration radii, a_1, a_2, and a_3 are mutually close, the M_4 is nearly tetrahedral. For the local equilibrium structure, it holds that $a_1=a_2=|a_3|=4.24$. On the other hand, the largest and the smallest gyration radii a_1 and a_3 deviate largely from their equilibrium values in the isomerizing motions, and a_3 reaches zero at an instant that the system crosses the so-called dividing surface at the transition state (planar structure). In this example, the isomerization reactions happened to take place three times. It is ob-

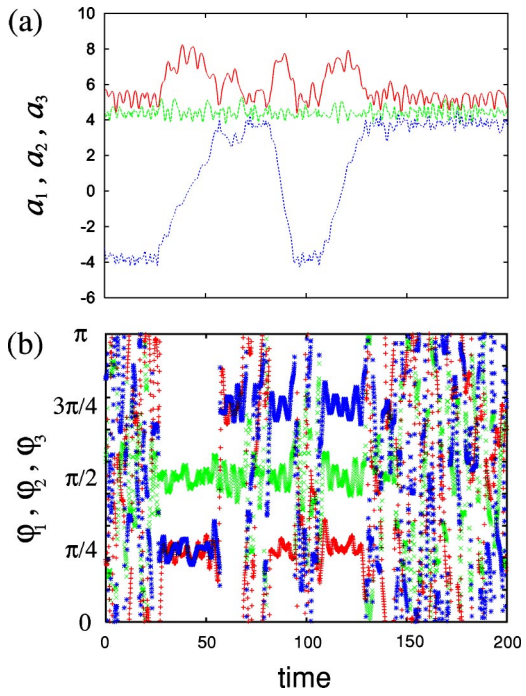

FIG. 13. (Color online) A typical time evolution of the internal variables for a four-atom cluster. Three gyration radii, a_1, a_2, and a_3 are shown ($a_1 \geqslant a_2 \geqslant a_3$) in panel (a), while (b) shows the three hyperangles, $\varphi_1(+)$, $\varphi_2(\times)$, and $\varphi_3(*)$. Structural isomerization reaction has occurred three times in this example by crossing the planar structures as indicated by the condition $a_3=0$. Total internal energy is $E=-3.91\varepsilon$.

served that the hyperangles vary rapidly when the system comes close to the equilibrium structure, while they are almost locked to certain values during the period of collective isomerization motions as will be seen later.

The origin of the rapid democratic rotations in the vicinity of the local equilibrium structures lies in the degeneracy among the three gyration radii there. Similarly to Eq. (36), the components of the democratic angular velocity $\gamma_{\alpha\beta}$ ($\alpha,\beta=1,2,3,\alpha\neq\beta$) are expressed as

$$\gamma_{\alpha\beta}=\dot{\boldsymbol{u}}_\alpha\cdot\boldsymbol{u}_\beta=\frac{\boldsymbol{u}_\alpha^T(\dot{\mathsf{W}}_s^T\mathsf{W}_s+\mathsf{W}_s^T\dot{\mathsf{W}}_s)\boldsymbol{u}_\beta}{a_\alpha^2-a_\beta^2}, \tag{62}$$

which suggests that the coupling between the two axes of the democracy frame, $\boldsymbol{u}_\alpha$ and $\boldsymbol{u}_\beta$, should be enhanced in the vicinity of the degeneracy $a_\alpha^2\approx a_\beta^2$. Another reason for the rapid democratic rotations comes from the flatness of the potential in the vicinity of the tetrahedral structure with respect to the democratic rotations, just as we have seen in Fig. 8 for the M_3 cluster.

The angles at which the hyperangles are locked are associated with the symmetry of molecular structure. For instance, the set of angles $(\varphi_1,\varphi_2,\varphi_3)=(\pi/4,\pi/2,\pi/4)$, which appears as the first reaction in Fig. 13, represents the symmetry of puckered rhombus (point group C_{2v}), as can be confirmed in Eq. (45). Projection of the M_4 cluster in this symmetry onto a plane perpendicular to the principal axis $\boldsymbol{e}_3$ leads to the planar rhombus. Of course, the M_4 cluster itself

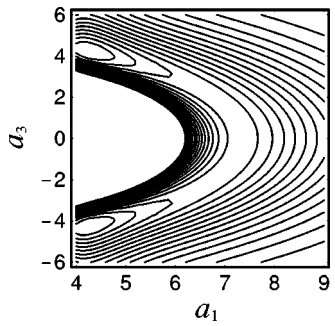

FIG. 14. Potential-energy surface on the a_1-a_3 plane fixing the remaining gyration radius $a_2=4.25$ and all the hyperangles to one of the sets given in Fig. 12. There exist local potential minima at (4.24,4.24) and (4.24,−4.24) which correspond to the permutationally distinctive tetrahedral structures. The saddle point is located at $(a_1,a_3)=(7.33,0)$ which corresponds to the rhombus-shaped structure. The energy difference between the neighboring contour lines is 0.278ε.

can be continuously deformed keeping the puckered-rhombus symmetry to the planar rhombus structure (point group D_{2h}), which is the saddle structure. Therefore the observed hyperangle locking during the periods of isomerizing motions indicates that the cluster undergoes the reactions nearly keeping the symmetry (puckered rhombus→planar rhombus→puckered rhombus). The set of locked angles is listed in Fig. 12. Although the locked angles depend on the choice of the Jacobi coordinates, the phenomenon of locking does not.

Figure 13 highlights that the collective variables dominating this isomerizing dynamics are the gyration radii a_1 and a_3, since a_2 and all the hyperangles do not vary much during the period of collective motion. Hence, a reaction path can be effectively described on the a_1-a_3 plane. In Fig. 14, we show the potential-energy surface on the a_1-a_3 plane fixing the remaining internal variables to values corresponding to the rhombus-shaped saddle structures; $a_2=4.25$ and all the hyperangles given in Fig. 12. On the a_1-a_3 plane in Fig. 14, two equilibrium points corresponding to the permutationally distinctive tetrahedral structures are connected by a curved reaction path which passes through a saddle point corresponding to the planar-rhombus structure. The isomerizing motion of the M_4 cluster proceeds overwhelmingly along this reaction path. As in the case of Fig. 7, the reaction path of Fig. 14 is closed as soon as the hyperangles deviate from the values listed in Fig. 12. In this way, hyperangles switch the reaction gate in the a_1-a_3 space.

D. Effects of DCF and trapped motion around the transition state

It is remarkable that isomerization of the M_4 cluster thus extracted on the a_1-a_3 plane is found to be quite similar to the dynamics of M_3 cluster. Therefore a_1 and a_3 are regarded as collective coordinates dominating dynamics in the six-dimensional internal space. Likewise, it is expected that the role of the DCF in the M_4 must be as crucial as that for the M_3. We next verify this presumption.

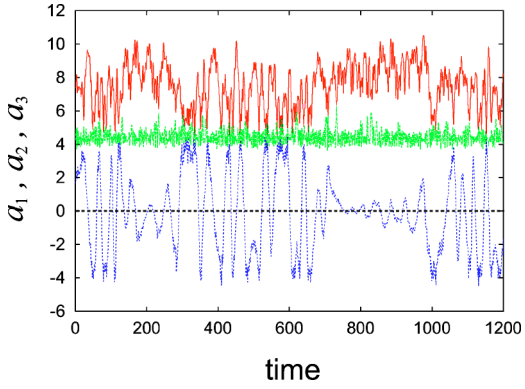

FIG. 15. (Color online) A typical time evolution of the gyration radii, a_1, a_2, and a_3 ($a_1 \geqslant a_2 \geqslant a_3$), showing the trapped motion around the planar saddle structure. The four-atom cluster stays in the region around the planar structure from $t \approx 150$ to $t \approx 300$ and from $t \approx 700$ to $t \approx 950$, recrossing the dividing surface several times. Total internal energy of the trajectory is $E = -3.06\varepsilon$.

In the motions in the vicinity of the tetrahedral structure, it is expected that the M_4 cluster always tends to be collapsed so as to avoid the degeneracy (coincidence) among the three gyration radii due to the strong DCF arising from the rapid democratic rotations seen in Fig. 13(b). Figure 14 suggests that the largest gyration radius a_1 must increase and the absolute value of the smallest gyration radius $|a_3|$ must decrease in order for the trajectory on the a_1-a_3 plane to proceed to the transition-state region. The DCF works to enhance this distortion: it tends to enlarge the largest gyration radius a_1 and to decrease the absolute value of the smallest gyration radius $|a_3|$, which are confirmed in Eqs. (57)–(59). Thus, it is again recognized that the DCF tends to push the M_4 into the reaction pathway in the a_1-a_3 space.

Just as the three-atom cluster, the M_4 often shows a trapped motion around the planar rhombus-shaped saddle structures. In Fig. 15, we show a typical example of the time-evolution of the three gyration radii, a_1, a_2, and a_3, in which the values of a_1 and $|a_3|$ are kept apart for a while without going to their equilibrium values. This clearly indicates that the M_4 cluster is trapped around the planar rhombus-shaped saddle structure and recrosses the potential barrier several times. The similar behavior is frequently observed especially at high internal energy. Again, this peculiar motion is attributed to the DCF. When a trajectory on the a_1-a_3 plane gets to the vicinity of the line $a_3 = 0$, that is, the vicinity of the transition states, the democracy frame oscillates slightly around one of the orientations specified by the hyperangles in Fig. 12 as we have seen in Fig. 13. These small oscillations generate DCF in the gyration space and can affect the behavior of trajectories on the a_1-a_3 plane. In particular, the two components of the DCF appeared in the right-hand side of Eq. (59), which are proportional to γ_{32}^2 and γ_{31}^2, always act on the smallest gyration radius, a_3, to diminish its absolute value. This means that these components of DCF can have an effect of trapping the system within the planar structure. In order to make this point more explicit, we define an effective potential V_{eff} regrouping the Lagrangian Eq. (56) as

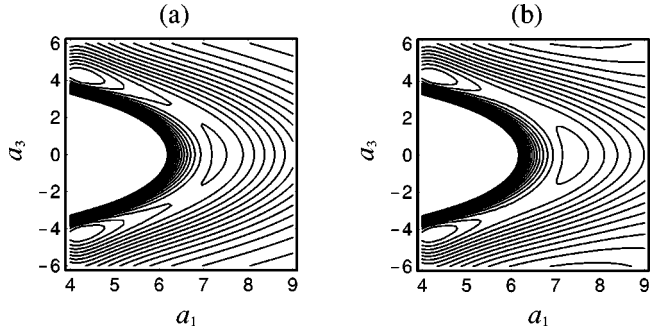

FIG. 16. Effective potential-energy surfaces, Eq. (63), on the a_1-a_3 plane fixing the remaining shape variables to the same values as in Fig. 14. (a) $\gamma_{12} = 0.05, \gamma_{23} = 0.1, \gamma_{31} = 0.05$. (b) $\gamma_{12} = 0.2, \gamma_{23} = 0.1, \gamma_{31} = 0.05$. The energy difference between the neighboring contour lines is 0.278ε.

$$V_{\text{eff}} = -\frac{(a_1^2 - a_2^2)^2}{2(a_1^2 + a_2^2)}\gamma_{12}^2 - \frac{(a_2^2 - a_3^2)^2}{2(a_2^2 + a_3^2)}\gamma_{23}^2 - \frac{(a_3^2 - a_1^2)^2}{2(a_3^2 + a_1^2)}\gamma_{31}^2 + V(a_1, a_2, a_3, \varphi_1, \varphi_2, \varphi_3). \tag{63}$$

A typical energy surface of the effective potential on the a_1-a_3 plane is shown in Fig. 16(a), where we have set the components of democratic angular velocity as $\gamma_{12} = 0.05, \gamma_{23} = 0.1, \gamma_{31} = 0.05$, and the remaining internal variables are fixed to the same values as in Fig. 14. We see that a basin structure of the effective potential certainly has appeared at the saddle point of the usual potential-energy surface $V(a_1, a_2, a_3, \varphi_1, \varphi_2, \varphi_3)$. This clearly accounts for the fact that the planar rhombus-shaped saddle structures are stable enough to allow for the relevant trapped motion. The components of the DCF proportional to γ_{12}^2 (or γ_{21}^2) do not act on the smallest gyration radius, a_3, directly but act on a_1 and a_2 to enlarge a_1 and to diminish a_2 [cf. Eq. (57) and Eq. (58)]. Therefore it is expected that the increase of γ_{12}^2 should have an effect of broadening the basin on the effective potential around the saddle point on the a_1-a_3 plane in the direction of positive a_1 axis. This effect can be observed in Fig. 16(b), where only the value of γ_{12} is increased to $\gamma_{12} = 0.2$ with other values fixed to the same values as in Fig. 16(a). In addition, it is also expected that the components of the DCF proportional to γ_{12}^2 should have an effect to further distort a trapped planar M_4 cluster into a linear structure.

V. CONCLUDING REMARKS

We have studied structural isomerization dynamics of three- and four-atom clusters using the PAHC to extract the effect of the intrinsic non-Euclidean metric inherent to the internal space. First, it has been revealed that the PAHC are quite effective to extract a few parameters that essentially dominate the collective isomerization dynamics. In both three- and four-atom clusters, it has turned out that the democratic rotation (changes of the hyperangles) switches reaction path in the gyration space, and only when the hyperangles are locked to certain appropriate angles, the gate for isomerization in the gyration space becomes open.

Second, we have extracted a metric force called DCF as an intrinsic factor to dominate the internal dynamics of *n*-body systems. The DCF arises as a consequence of the democratic rotations and works in the gyration space. We have shown that the DCF is of comparable magnitude with the usual potential force and thereby plays important roles in the collective motions of clusters. In general, the DCF acts on the gyration parameters (gyration radii) to avoid degeneracy between them. That is to say, the DCF generally tends to distort the three- and four-atom clusters so as to be more massive in the massive direction and to be less massive in the less massive direction. As a result, the vicinity of the local equilibrium structures where gyration radii are degenerate tends to be avoided (less frequently visited) in their dynamics, although this fact is not in harmony with our intuition. In this sense, the DCF tends to induce another kind of symmetry breaking [27] associated with the degeneracy. We have found that the present asymmetry among the gyration radii induced by the DCF helps the clusters to proceed to the reaction pathway in the gyration space.

Furthermore, we have shown that the motions around the transition states of the three- and four-atom clusters are dynamically stabilized by the DCF. The origin of this phenomenon has been visually clarified by demonstrating the newly appearing basin at the transition state in the gyration space. Because of this basin, the clusters can stay long and thereby recross the dividing surfaces. Our approach has clarified quantitatively the manner of competition between the ordinary force arising from the static potential and the kinematic force.

Finally we would like to emphasize again that molecular motion is subject to a significant kinematic force arising from the DCF, even if it is free of a potential function. To the best of our knowledge, the importance of this kind of kinematic force has not been fully appreciated before in the conventional reaction-rate theories, which are based mostly on the topography of potential surfaces. Our theoretical development has provided a different view of the mass effects. Since the concept of internal space, gauge-invariant metric tensor on it, democratic rotations, and the DCF, are all common to general many-body systems, such as nuclear systems, polymers, celestial systems, and so on, irrespective of the individually working interaction potentials, the DCF can generally be responsible for an important part of internal motions.

ACKNOWLEDGMENT

This work was supported in part by the Grant-in-Aid from the Ministry of Education, Culture, Sports, Science and Technology of Japan.

[1] R.S. Berry, T.L. Beck, H.L. Davis, and J. Jellinek, Adv. Chem. Phys. **70**, 75 (1988); J. Jellinek, T.L. Beck, and R.S. Berry, J. Chem. Phys. **84**, 2783 (1986); F.G. Amar and R.S. Berry, *ibid.* **85**, 5943 (1986).

[2] P. Labastie and R.L. Whetten, Phys. Rev. Lett. **65**, 1567 (1990).

[3] C. Amitrano and R.S. Berry, Phys. Rev. Lett. **68**, 729 (1992); Phys. Rev. E **47**, 3158 (1993).

[4] R.J. Hinde and R.S. Berry, J. Chem. Phys. **99**, 2942 (1993); R.J. Hinde, R.S. Berry, and D.J. Wales, *ibid.* **96**, 1376 (1992).

[5] T. Komatsuzaki and M. Nagaoka, J. Chem. Phys. **105**, 10838 (1996); T. Komatsuzaki and R.S. Berry, *ibid.* **110**, 9160 (1999); **115**, 4105 (2001).

[6] R.S. Berry, Chem. Rev. (Washington, D.C.) **93**, 2379 (1993); P.A. Braier, R.S. Berry, and D.J. Wales, J. Chem. Phys. **93**, 8745 (1990); M.A. Miller, J.P.K. Doye, and D.J. Wales, *ibid.* **110**, 328 (1999).

[7] C. Seko and K. Takatsuka, J. Chem. Phys. **104**, 8613 (1996); **108**, 4924 (1998); **109**, 4768 (1998); K. Takatsuka and C. Seko, *ibid.* **105**, 10356 (1996); **110**, 3263 (1999); T. Yanao and K. Takatsuka, Chem. Phys. Lett. **313**, 633 (1999); K. Takatsuka and T. Yanao, J. Chem. Phys. **113**, 2552 (2000).

[8] J. I. Steinfeld, J. S. Francisco, and W. L. Hase, *Chemical Kinetics and Dynamics* (Prentice-Hall, Englewood Cliffs, New Jersey, 1989).

[9] W.H. Miller, J. Phys. Chem. A **102**, 793 (1998); Faraday Discuss. **110**, 1 (1998)

[10] R. Montgomery, in *The Geometry of Hamiltonian Systems*, edited by T. Ratiu (Springer-Verlag, Berlin, 1991), p. 403.

[11] R.G. Littlejohn and M. Reinsch, Rev. Mod. Phys. **69**, 213 (1997).

[12] A. Guichardet, Ann. Inst. Henri Poincare **40**, 329 (1984).

[13] A. Tachibana and T. Iwai, Phys. Rev. A **33**, 2262 (1986).

[14] T. Iwai, Ann. Inst. Henri Poincare **47**, 199 (1987); J. Math. Phys. **28**, 964 (1987); **28**, 1315 (1987); Phys. Lett. A **162**, 289 (1992).

[15] F.T. Smith, J. Math. Phys. **3**, 735 (1962); Jean-Mark Lévy-Leblond and Monique Lévy-Nahas, J. Math. Phys. **6**, 1571 (1965); R.C. Whitten and F.T. Smith, *ibid.* **9**, 1103 (1968); A. Kupperman, Chem. Phys. Lett. **32**, 374 (1975); B.R. Johnson, J. Chem. Phys. **73**, 5051 (1980); A. Novoselsky and J. Katriel, Phys. Rev. A **49**, 833 (1994).

[16] C. Eckart, Phys. Rev. **46**, 383 (1934).

[17] X. Chapuisat and A. Nauts, Phys. Rev. A **44**, 1328 (1991).

[18] X. Chapuisat, Phys. Rev. A **45**, 4277 (1992).

[19] X. Chapuisat, J.P. Brunet, and A. Nauts, Chem. Phys. Lett. **136**, 153 (1987).

[20] A. Kuppermann, J. Phys. Chem. A **101**, 6368 (1997).

[21] R.G. Littlejohn and M. Reinsch, Phys. Rev. A **52**, 2035 (1995).

[22] R.G. Littlejohn, K.A. Mitchell, V.A. Aquilanti, and S. Cavalli, Phys. Rev. A **58**, 3705 (1998).

[23] R.G. Littlejohn, K.A. Mitchell, M. Reinsch, V. Aquilanti, and S. Cavalli, Phys. Rev. A **58**, 3718 (1998).

[24] R.S. Berry, J. Chem. Phys. **32**, 933 (1960).

[25] *Geometric Phases in Physics*, edited by A. Shapere and F. Wilczek (World Scientific, Singapore, 1989).

[26] J.W. Zwanziger, M. Koenig, and A. Pines, Annu. Rev. Phys. Chem. **41**, 601 (1990).

[27] I.B. Bersuker, Chem. Rev. (Washington, D.C.) **101**, 1067 (2001).
[28] J. Costley and P. Pechukas, J. Chem. Phys. **77**, 4957 (1982).
[29] J. Manz, E. Pollak, and J. Römelt, Chem. Phys. Lett. **86**, 26 (1982).
[30] V. Aquilanti and S. Cavalli, J. Chem. Phys. **85**, 1355 (1986).
[31] G. Strang, *Linear Algebra and its Applications* (Academic Press, New York, 1976).
[32] H. Goldstein, *Classical Mechanics* (Addison-Wesley, New York, 1980).